Aerodynamical and sonic boom optimization of a supersonic aircraft

M. Vázquez, Alain Dervieux, B. Koobus

INRIA

INSTITUT NATIONAL DE RECHERCHE EN INFORMATIQUE ET EN AUTOMATIQUE

Aerodynamical and sonic boom optimization of a supersonic aircraft

M. Vázquez A. Dervieux B. Koobus

N° 4520

July 17th, 2002

THÈME 1

ISSN 0249-6399 ISRN INRIA/RR--4520--FR+ENG

INRIA
SOPHIA ANTIPOLIS

Aerodynamical and sonic boom optimization of a supersonic aircraft

M. Vázquez* A. Dervieux† B. Koobus‡

Thème 1 — Réseaux et systèmes
Projet Tropics

Rapport de recherche n° 4520 — July 17th, 2002 — 38 pages

Abstract: Sonic Boom Reduction will be an issue of utmost importance in future supersonic carriers, due to strong regulations on acoustic nuisance. The present work introduces a technique for optimizing the aerodynamical performance *and* the sonic boom production, through optimal shape design. Based in a so-called CAD-free parametrization method, which relies on the *discretized shape* by working in a parameter space determined by the skin nodes physical location, this methodology introduces several distinctive features. First, an additive multilevel optimization preconditioner is designed, which both smoothes the iterated shape and speeds up the optimization convergence. Second, the sonic boom is reduced indirectly by reducing what we call the *sonic boom emission*. Third, an ad-hoc simple cost functional is constructed which considers both aerodynamical parameters and sonic boom emission.

Key-words: Computational fluid dynamics - Shape optimal design - Gradient method - Shape parametrization - Steepest descent - Optimization - Multilevel optimization - Adjoint methods - Euler equations - Unstructured mesh - Transpiration conditions

* INRIA, 2004 Route des Lucioles, BP. 93, 06902 Sophia-Antipolis, France
† INRIA, 2004 Route des Lucioles, BP. 93, 06902 Sophia-Antipolis, France
‡ Université de Montpellier II, Dept Mathématiques, CC.051 34095 MONTPELLIER Cedex 5

Unité de recherche INRIA Sophia Antipolis
2004, route des Lucioles, BP 93, 06902 Sophia Antipolis Cedex (France)
Téléphone : +33 4 92 38 77 77 — Télécopie : +33 4 92 38 77 65

Optimisation de l'aérodynamique et du bang sonique pour un avion supersonique

Résumé : La réduction du bang supersonique va prendre une importance de plus en plus grande pour les futurs avion supersoniques sous la pression de fortes réglementations sur la nuisance qui en résulte. Ce travail décrit une technique d'optimisation à la fois des performances aérodynamiques et de la production du bang supersonique par l'optimisation de forme. Cette méthodologie est basée sur un paramétrage sans CAO, puisqu'elle modifie la forme discrète en travaillant sur la position des nœuds de la peau du maillage. Elle présente les spécificités suivantes. Tout d'abord, nous définissons un préconditionneur d'optimisation de type multiniveau additif. Il régularise la forme itérée et accélère la convergence. Ensuite, nous construisons une fonctionnelle coût prenant en compte les coefficients aérodynamiques et l'émission du bang supersonique.

Mots-clés : Mécanique des Fluides Numérique - Optimisation de forme - Méthode de gradient - Paramétrisation de forme - Plus grande descente - Optimisation - Optimisation multi-niveau - Équations d'Euler - Maillage non-structuré - Conditions de transpiration

1 Scope of the paper

Optimal shape design in aerodynamics is reaching maturity and will reach in the next years the point where best analysis codes (Navier-Stokes) will be involved in a loop optimizing thousands of shape parameters. Since both parameters and flow variables will be represented by a large number of unknowns, it becomes important to derive efficient solution/optimization methods with low complexity when the number of variables is increased.

We observe that the complexity question of flow solutions is adressed by many works, with some success when Multi-Grid algorithms or Domain Decomposition Methods are used: these algorithms enjoy a convergence rate that does not degrade when the number of unknowns is increased. Analogously, we concentrate in this paper on the optimization problem and we look for algorithms that would also have a convergence rate insensitive to the number of optimization parameters.

One essential option in this direction is to compute sensitivity, that is the derivative of certain quantities (at least the functional to minimize) with respect to a set of parameters. Most minimization processes rely on sensitivity, but when the variations are computed by divided differences, the computational cost will probably exceed n times the cost of one functional where n is the number of parameters. Contrarily, solving an adjoint system for computing the gradient of the functional is no more costly than computing only one functional while it provides information for all of the n optimization parameters. This point of view is not new (see for example [15]), but it is still facing some practical problems in writing the differentiated code. One answer is automated or assisted differentiation ([4],[26]). By differentiation (automated or by hand), large 3D geometries with the Euler flow model could be handled with a "CAD-free" parametrization. By "CAD-free", according to [21], we mean that the shape is represented only by a numerical technology, typically the boundary of the mesh used for solving the CFD problem. A pioneering work using this option is [25].

A second path to less costly optimization allowed by the derivation of an adjoint system is to simultaneously solve the combination of state system (the flow), adjoint system, and optimality equation related to the gradient of functional. This is suggested by Ta'asan et al., called "one-shot" method [13].

In [18], it is proposed to combine the one-shot method with a V-cycle multilevel parametrization of the control variable. It is a method relying on a gradient approach, applied to the **unstructured** representation of a shape as the skin of a 3D tetrahedrization. For multi-levelling, the volume-agglomeration principle introduced in [14] is applied. The V-cycle method works successively in one cycle into the different available levels, so that the cost of one cycle is proportional to the number of level. On the contrary, in [5], the authors showed that in the case of embedded levels, multi-grid convergence can be obtained by replacing any cycle by a single correction step if we can use a multi-level preconditionner. In [24], a family of such multi-level preconditioners are derived for unstructured meshes, particularly important for complex geometries like those we are dealing with.

The purpose of this paper is double. Firstly and following this last line, to extend the Marco-Koobus-Dervieux preconditioner to the parametrisation of "CAD-free" 3D shapes.

And secondly, to apply an optimization loop using this preconditioner to the optimisation of the aerodynamics and sonic boom of a supersonic aircraft.

Let us introduce this idea. Any solid body moving at supersonic speeds developes a shock wave system. A simple solid of revolution (like a projectile) produces only two shock waves, one in front and the other one behind. Although more complex bodies, like planes, produce more complex shock patterns, these patterns can coalesce beyond the near field. Figure 1 sketches the situation. Once the shock wave pattern reaches the soil, it has ultimately became an two-shock system, a so-called N-type pressure wave, which is dragged by the plane movement. Both the pressure initial rise and final drop are steepened after propagation through the atmosphere, producing very strong explosive sounds on the ground, which for instance lays at 15km below the airplane for the Concorde flying at cruise altitude. This fact has motivated the prohibition of Concorde supersonic flights over land. Therefore, the reduction of the sonic boom is an important issue in the specification or the next generation of supersonic aircrafts [16, 27]. According to [27], sonic boom minimization could be attained considering basically three points: to get the minimum pressure impulse, which is defined as the integral of the overpressure signature, or the minimum initial shock pressure rise or finally to smooth the pressure rise by distributing it in a longer rise time. Different optimization strategies focus on one or several of these possibilities.

The paper is organized as follows :

First, we introduce the problem and sketch the lines motivating this work. Then we present the multilevel parametrization and preconditioner we propose for 3D shape optimization. It follows a deeper description of the optimization problem to solve the corresponding optimality conditions. Numerical experiments related to aerodynamical performances and sonic boom reduction for a supersonic aircraft are then reported. Finally, some conclusions are drawn.

2 Problem statement

2.1 The optimization problem. Adjoint formulation

The general form of the problem to solve is the following: we want to find γ_0 that minimizes a certain functional $j(\gamma) = J(\gamma, W(\gamma))$ under the constraint $\Psi(\gamma, W(\gamma)) = 0$. All γ's represent the parametrization of the shape to optimize. $j(\gamma)$ is the cost functional, its dependence on γ is set by the aerodynamicist according to his needs. Finally, the constraint $\Psi(\gamma, W(\gamma)) = 0$ is the set of flow equations themselves, in this case the compressible Euler equations, solved in a domain Ω, for which $\partial\Omega \supset \gamma$. $W(\gamma)$ is the flow field.

The minimization problem is then solved using Lagrange multipliers. The problem's Lagrangian is

$$L(W(\gamma), \gamma, \Pi(\gamma)) \;=\; J(W(\gamma), \gamma) + \langle \Psi(\gamma, W(\gamma)), \Pi(\gamma) \rangle, \tag{1}$$

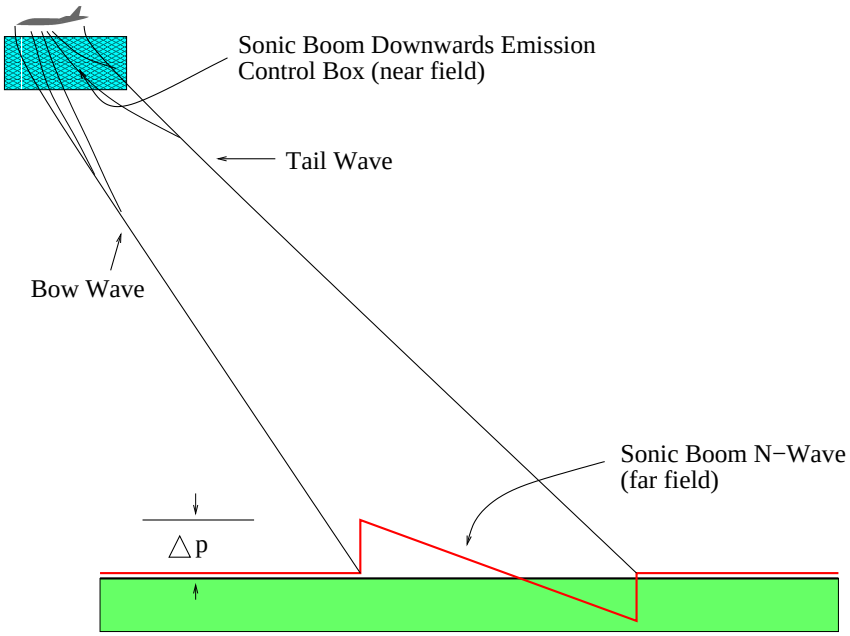

Figure 1: The sonic boom. Sketch of near and far field shock wave patterns of a supersonic aircraft.

where $\Pi(\gamma)$ is a generalized Lagrange multiplier, and $\langle\ ,\ \rangle$ is a suitable scalar product. Then, γ_0 will be find after solving

$$\begin{aligned}
&\Psi(\gamma, W(\gamma)) = 0 \\
&(\nabla_w \Psi(\gamma, W(\gamma)))^* \ \Pi = \nabla_w J(\gamma, W(\gamma)) \\
&j'(\gamma) = \nabla_\gamma J(\gamma, W(\gamma)) \quad - \quad \langle \Pi(\gamma), \nabla_\gamma \Psi(\gamma, W(\gamma)) \rangle.
\end{aligned} \tag{2}$$

The first line is the flow solution, to obtain $W(\gamma)$. The second one is the so called adjoint flow solution, to get $\Pi(\gamma)$. And in the last line, the gradient $j'(\gamma)$ of the cost functional is evaluated, which in turn will be used to modify the former γ. The derivatives of both the constraint and the cost functional can be obtained either by finite differences or, much more efficiently, by automatic differentiation [21]. We propose below how to adapt this technique to the sonic boom optimization problem.

2.2 Sonic boom optimization

The main point in sonic boom reduction is that it has to be attained without a prohibitive degradation of the aircraft aerodynamical performance. Furthermore, a direct evaluation

of the shock signature on the soil from the 3D Euler equations is computationally out of reach. It is necessary to model the far field sonic boom propagation, an issue authoritatively described both in [16] through the pioneering works of Witham about the matter, or in [27]. The central idea in Witham's theory is to propagate bi-dimensionally, in a plane spanned by the flight direction and the vertical one, the near field shock wave pattern, assuming some (indeed strong) hypothesis. This makes the pressure soil signature evaluation a problem separated from the CFD simulation: it is a combination of a linearized propagation theory for the far field signature and a non linear three dimensional set of equations (Euler's or Navier-Stokes') for the near field flow.

We have identified two recent leading works on sonic boom optimization which follow this line. One alternative is presented in [9]. In this work, it is proposed a parametrical optimization scheme for the sonic boom, where the parameters space is determined by several position coordinates of flying appendages (like canards) and nose tilting. The signature is modelled by the linearized theory as a function of some geometric aircraft parameters. In the reduced design parameters' space, an adjoint flow problem is solved in order to compute the cost functional gradient. The problem then results in a minimization of only the initial shock pressure rise (ISPR), **leaving aside any reduction of the rest of the shocks present in the signature**. The other alternative is to increase the parameters space by taking a finer parametrization of the *shape* itself of the wings and/or appendages: in [23, 1] an adjoint method is again used to optimize a model supersonic aircraft by modifiying the positions of the discretized skin mesh (in [21], this kind of shape parametrization is christened **"CAD-free"**, conversely to the **"CAD-based"** parametrization like that of [9], which uses a reduced parameters space. We will follow this nomenclature too). In this case also, the pressure far field is computed, but now as function of the near field pressure and as a result of an inverse problem **given a target pressure ground signature**. This is done by solving two coupled adjoint problems. Within this general line is also [28], as cited in both [23] and [9], but instead of solving the adjoint problem, these researchers use a genetic algorithm approach.

In the present work, we propose a different, yet simplified way of sonic boom optimization. Assuming that the source of the pressure signature on the soil is the near field shock pattern below the airplane (we call it the **sonic boom downwards emission**, SBDE), by reducing it, the pressure signature will be consequently reduced. In this way, the far field could then be evaluated but out of the optimization cycle, just to check the results. The SBDE can be quantified as the pressure gradient squared norm integrated in a given "control box" below the airplane and neighboring it, which is in fact a part of the CFD domain. The first obvious idea is to consider it as the cost functional to try to minimize (additionally to some other terms depending on the aircraft performance parameters like lift or drag). Although we think that this could be further improved, we have left this for future works, restraining us to this first idea for the rest of the paper. The final goal is then to optimize the wings, nose, appendages and other aircraft parts by changing their shapes, under a "CAD-free" scheme, and following the theoretical lines depicted below, among them the additive multilevel preconditioner or the transpiration conditions. The outcome will be shapes that produce **the least possible**

SBDE while keeping good flight performance and realistic constructive features (like wing thickness, for instance). Another novel "CAD-free" approach is that of [20].

It is worth to mention a basic difference relative to all the alternatives referenced above. While in [23, 1], a target far field pressure distribution is given, in [9], the goal is to minimize only the ISPR. In the former case, the optimization is done over the shape of the complete aircraft and in the latter in a reduced design parameters space. In both cases, there is a sort of additional constraint in the minimization problem, imposed by limiting the space where to look for the solutions: either giving a target pressure or focusing only in the ISPR. We believe that sometimes and depending on what is the goal on demand, this approach can be very convenient. However, our analysis is free of this constraint: we want to minimize the near field SBDE and see what we get, on the conviction that new aerodynamical shapes can be found, arising from the proposed minimization problem and retaining good flight performance. We think that our approach is neither better nor worse, but complementary to other kind of approaches. Another important difference is that all the works previously mentioned attack directly the full aircraft problem. Here, we start by optimizing *isolated* parts of the plane, because we think that this can lead to a deeper study about what is really producing the sonic boom. For instance, in the case of the Supersonic Business Jet, we have observed the effect of the dual-sweep angle wings. We therefore have proceeded by firstly analyzing simple forms, followed by individual parts of an aircraft, either integrated to or separated from the aircraft. The final stage (being done while this report is in print) is to carry out the full optimization of the plane.

3 Multilevel optimization

We turn now to the first focus of this paper, *the application of an additive multilevel optimization algorithm to the optimization of 3D surfaces.* This rely on an adequate multilevel parametrization. Recall that we consider the minimization problem:

$$\text{Find } \bar{u} \in V \quad \text{such that} \quad \bar{u} = \arg\min_{u \in V} j(u) \tag{3}$$

where V is a Hilbert space (think of a Sobolev space) and where the cost functional j is continuously differentiable in the Hilbert space V. We investigate the application of the multilevel optimization to Problem (3) in order to put in evidence the basic options that will allow to obtain a multilevel solution in an efficient way, with the aid of a certain parametrization of the shape. This is deeply described in references like [19] or [8]. We start by explaining the multilevel parametrization with the aid of functions defined on the 2D plane.

3.1 2D case

Let us write a *coarse level correction* as follows:

$$u_{2h}^{n+1} = u_{2h}^{n} - \rho_{opt}\ \mathcal{L}\mathcal{P}\mathcal{P}^{*}\mathcal{L}^{*}\ j'(u_{2h}^{n}). \tag{4}$$

In the above expression, the linear operators $\mathcal{L}$ and $\mathcal{P}$ are projections to a smaller space, that are defined below; u_{2h} is the discretized value of u on the coarse mesh. A key condition for efficiency is that the fixed point u^*_{2h} of (4) do satisfy $\mathcal{L}\mathcal{P}\mathcal{P}^*\mathcal{L}^*\ j'(u^*_{2h}) = 0$, i.e. it is a *convergent approximation* of "arg min j" when the mesh size is increased; in other words:

$$u^*_{2h} \quad \longrightarrow \quad \bar{u} \text{ in } V \quad \text{as} \quad h \to 0 \tag{5}$$

In (4), $\mathcal{P}$ is a prolongation operator from coarse level to fine level and its transpose $\mathcal{P}^*$ is a restriction operator from fine level to coarse level. $\mathcal{L}$ is an average smoothing operator ($\mathcal{L}^*$ is its transpose) defined by :

$$(\mathcal{L}u)_i = (1-\theta)u_i + \theta \ \frac{\displaystyle\sum_{j\in\mathcal{V}(i)\cup\{i\}} Area(j)\ u_j}{\displaystyle\sum_{j\in\mathcal{V}(i)\cup\{i\}} Area(j)} \tag{6}$$

where j runs over the $\mathcal{V}(i)$ cells neighboring i and $Area(j)$ is the area of each of them built around vertices with the triangle medians.

3.2 Parametrization of 3D surfaces

We now consider the parametrization for optimizing an aircraft in a 3D Euler flow. The parametrized shape is then a 3D surface and flow calculations are performed on an unstructured 3D mesh. The building of a multilevel parametrization [3] of this shape will rely on a node-agglomeration principle (see [18]). The surface is assimilated to a manifold Σ, that is smooth enough. A deformation produced on its discretization Σ_h, is noted $\delta\Sigma_h$; the new manifold $\Sigma_h + \mathcal{L}\mathcal{P}\mathcal{P}^*\mathcal{L}^*\delta\Sigma_h$ is built by a projection $\mathcal{P}^*$ to a coarser level, a prolongation $\mathcal{P}$, transpose of $\mathcal{P}^*$, to the initial level, combined with an operator $\mathcal{L}$ (details are given in [18]). The smoothing operator $\mathcal{L}$ is an average weighted by a scalar product of normals :

$$(\mathcal{L}\ \vec{x})_i = (1-\theta)\vec{x}_i + \theta \ \frac{\displaystyle\sum_{j\in\mathcal{V}(i)\cup\{i\}} w_{ij}\vec{x}_j}{\displaystyle\sum_{j\in\mathcal{V}(i)\cup\{i\}} w_{ij}} \tag{7}$$

where w_{ij} are the weights defined by :

$$w_{ij} = \max\ (Area(i)\cdot Area(j)\cdot\vec{n}_i\cdot\vec{n}_j\ ,\ 0) \quad \|\vec{n}_i\| = 1\ \ \forall\ i \tag{8}$$

where θ is the smoothing parameter. Again $\mathcal{V}(i)$ represents the neighbors of cell i.

The above geometry is the surfacic boundary of a 3D unstructured tetrahedrization.

With the above transfer and smoothing operators from any level $m-1$ to level m as elementary bricks, we can derive a projection operator related to level k:

$$P_k \quad = \quad \prod_{1\le m\le k} \mathcal{L}_m\mathcal{P}_m\mathcal{P}^*_m\mathcal{L}^*_m \tag{9}$$

3.3 Multilevel preconditioner and optimization

In a way analog to [5], we introduce the multilevel preconditioner as follows:

$$P^* g \;=\; P_n g \;-\; \sum_{k}^{n-1} \frac{1}{4^{n-k}} \left(P_{k+1} g \;-\; P_k g\right) \tag{10}$$

where n is the coarsest level, and $g(\gamma, W, \Pi)$ is a function of variables γ,W and Π , that is identical to $j'(\gamma)$ only if $W = W(\gamma)$ (solution of state equation) and $\Pi = \Pi(\gamma)$ (solution of adjoint state equation). The multilevel gradient approaches considered here rely on the following algorithm:

Multilevel Preconditioned Algorithm:

`Do` nc

- `Compute state` W `and adjoint` Π`, compute the gradient` $g(\gamma^{nc}, W, \Pi)$
- `Compute the preconditioner` P^*
- `Compute` ρ `(internal cycle)`
- `Update the shape correction:`

$$\gamma^{nc} \;=\; \gamma^{nc-1} - \rho \quad P^* \;\; g(\gamma^{nc}, W, \Pi)$$

`Next` nc

The parameter ρ is either fixed or defined by a 1D search (steepest descent). This algorithm results in a *gradient method* when g is exactly $j'(\gamma)$, which is a descent one in a weak sense since the preconditioner is symmetric. We have seen that an additional smoothing, applied on $P^* \;\; g(\gamma^{nc}, W, \Pi)$ can indeed improve the solution, specially when the skin mesh that covers the shape to discretize is rather coarse or have acute edges. It is enough a single iteration of a Least Squares Smoothing [12] or simply the average smoothing operator defined in (6) with $\theta = 1$.

Conversely, when W and Π are obtained by applying only a few iterations of state equation and adjoint state equation iterative solution, g is not the gradient of j, but aims to converge towards $j'(\gamma)$ when the whole loop is converging; we refer to this algorithm as a **one-shot method** (according to [13]) for solving the optimality system of the optimization problem [17]. The performances of this approach for 2D applications are discussed in [10].

4 Application to 3D aerodynamics

4.1 Global approach. Transpiration conditions

The numerical method applied for predicting steady Euler flows, is a finite volume scheme. The numerical flux evaluation is done following one of these methods: Roe's or Van Leer flux vector splitting. The choice depends on factors like robustness or problem size. The overall differentiability of the process will allow to apply an exact-gradient approach. The application of a shape design loop should involve the repeated rezoning of the mesh to account for the modification of the shape of the aircraft. In this work, inspired by the approach used by Young *et al.* ([11]), we consider in a first phase the option of representing the shape modification by applying a transpiration condition; this means that the current shape is defined with respect to the mesh skin as a perturbation simulated by transpiration (see for example [22]), referred in the sequel as the "*transpired perturbation*". Then γ is the perturbation function; it is the algebraic length of the displacement of the boundary along its normal. We recall the transpiration condition for Euler flows: Let us denote by *shell* the shape to be emulated by transpiration and by $\vec{n}_{shell}$ the normal of the shell. The slip boundary term of the flux $\Psi(W)$ is defined as follows: for each component of the Euler flow equations set,

$$\Psi(W)_{slip\ boundary} = q\ W\ +\ (\,0\,,\,p(W)\ n_x\,,\,p(W)\ n_y\,,\,p(W)\ n_z\,,\,p(W)\ q\,) \tag{11}$$

where

$$q = \vec{V}\ .\ (\vec{n} - \vec{n}_{shell})$$

where $\vec{V}$ is the velocity of the fluid. This approximation has proved to be enough accurate for rather large perturbations of the boundary and very robust.

The sensitivity analysis has been exactly derived, but again in a first phase, only up to the first-order accurate upwind scheme. The validation of this sensitivity is performed by a direct comparison with divided differences of the cost function; error in gradient components is about .001.

The global scheme is essentially made of three loops. The external loop is a remeshing loop in which a new shape is derived from an old one updated by the transpired perturbation. In the examples presented here, as the grid movements where not so important, this remeshing step is skipped. However, it is worth to say that this was used to assess the correctness of the transpiration approach. In all of the cases that we have tested it, the flow field obtained either with transpiration or remeshing using as skin mesh that is produced by transpiration were basically the same. The extensive use of the outer remeshing loop is discussed in a forthcoming paper, where aeroelastic coupling is addressed and remeshing becomes a must.

The medium loop is a gradient optimization one in which the control variable is the transpired perturbation; this loop involves the evaluation of the gradient of the cost functional through an adjoint state. We have discussed in detail in previous works (e.g. [18]) the ability of the multilevel to converge with a speed that is rather insensitive to the number

of parameters; we now stress that, although easily obtained by the multilevel method, the optimal control can show spurious high frequencies. We think that the origin of an odd-even decoupling lies in the fact that normal vectors at nodes are (arithmetic) means of normal vectors to faces of the shape. From this point of view, the Euler flow is rather insensitive to high frequency oscillations of the boundary. This defect is amplified by the transpiration formulation in which high frequencies affect normals but not cell volumes! Our answer to this problem is either to avoid the use of the finest level, (which involves the whole set of boundary node coordinates) in the case of multilevel optimization, or, for the multilevel additive preconditioner, to smooth the normals. The most internal loop is the 1D local search of the steepest descent parameter ρ_{opt}. It is "local" in the sense that it is evaluated for each discretization level, only once in the case of the additive multilevel preconditioner. A future improvement of the algorithm will include a second order scheme and a trust-region minimization.

4.2 Volume preserving gradient projection

As a simple technique to approximately preserve the volume that is contained by the optimized shapes, once the gradient $g(\gamma, W, \Pi)$ is evaluated and before any other treatment (like smoothing or multilevel preconditioning) we proceed to project it on the space of volume preserving gradients. This is done as follows. For each of the skin mesh nodes i, whose physical position defines the parameter's space, assign

$$g(\gamma, W, \Pi)_i = g(\gamma, W, \Pi)_i - \frac{\sum_{j}^{N(i)} Area_j \; g(\gamma, W, \Pi)_j}{\sum_{j}^{N(i)} Area_j}. \tag{12}$$

In order to avoid volume "migration" from one end to the other of the optimized shapes, the whole volume is divided in transversal sections. Each node i can be therefore assigned to a section which contains $N(i)$ of them. Then, the volume is preserved locally for each section.

4.3 Sonic boom downwards emission optimization

We propose here to measure the sonic boom emission evaluating the volume integral of the squared pressure gradient in a control volume below the object. This it is integrated in the cost functional as follows:

$$j(\gamma) = \alpha_1 (C_D - C_D^{target})^2 + \alpha_2 (C_L - C_L^{target})^2 + \alpha_3 \int_{\Omega^B} |\nabla p|^2 \, dV \tag{13}$$

where α_1, α_2 and α_3 are constants that allow to vary the relative weight between the three constraints in $j(\gamma)$ that we want to consider, which are related to the aerodynamical

performance: drag, lift and sonic boom emission. The integration volume Ω^B is the part of the computational domain placed below the airplane, limited in its upper boundary by a plane like that of Figure 11.

In order to gain insight on what we propose, let us analyse a simple bi-dimensional example, derived from the ONERA M6 optimization that will be discussed later. Let us consider its mid wing-span vertical section as shown in Figure 6. We will take them as bi-dimensional airfoils for both the original and the optimized wings (that of Figure 6, bottom). We calculate then the supersonic flow around them (same Mach number and incidence angle as in the full M6 below) constructing an ad-hoc 2D discretization to propagate downwards the shock wave, vertically down to 10 times the chord approximately. This simplified example can help us to understand the dynamics of shock propagation for a given profile and its optimized counterpart, that has been derived following the scheme here proposed. It has to be said that the airfoils so obtained present a somewhat wrinkled profile because of the cutting process of the original rather coarse M6 skin mesh (see Figure 5) and not at all due to the optimization process itself.

The pressure contours for both the original and the optimized airfoils are shown in Figures 2 and 3. The downwards shock propagation can be clearly seen in Figure 2 and its spatial evolution in Figure 4, which represents the pressure at three different vertical positions: 0.5, 3 and 6 chord lenghts below the airfoil. By watching these figures, one can understand what kind of profiles we are looking for:

- The near field pressure peak has clearly diminished. This is attained by making a more acute leading edge with a flattened downards face.
- The pressure peak has been initially distributed in a wider area, by flattening the downwards face and slightly twisting the trailing edge, creating a sort of flap. This will also maintain the lift coefficient, as seen in Table 1.
- The small shock produced by the twisted trailing edge has a very important function: it has helped to quickly focalize the sharp first compression, but *whith no over-expansion behind it.*
- The last vertical position registered in Figure 4 lies at about 6 chord lenghts below the airfoils, equivalent approximately to a distance of 10 chord lenghts measured from the profiles to the propagated shock. There, while the original profile has developed the typical N-shape pressure distribution, the optimized one has a smaller pressure peak, a smaller pressure impulse (the integral of the pressure over the value at infinite [27]) and no overexpansion following the first peak.

We believe that the combination of all these effects will effectively reduce the far field sonic boom in a way (up to our knowledge) not studied before.

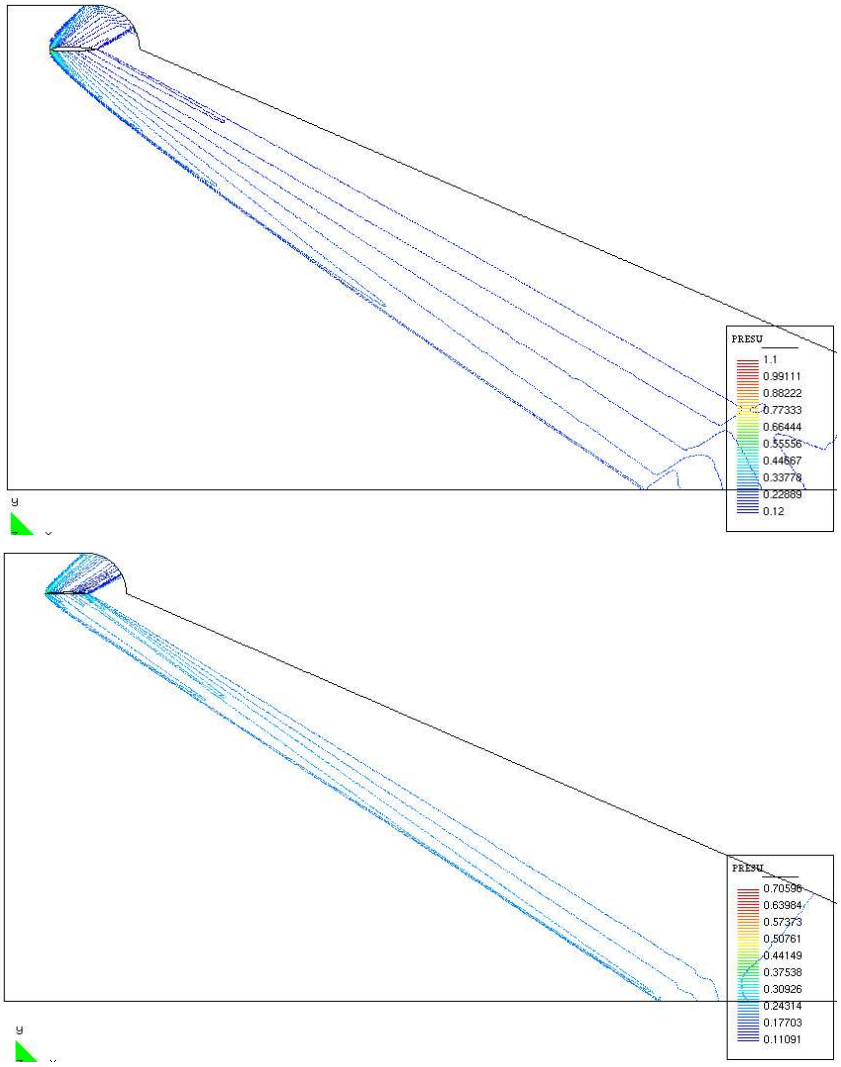

Figure 2: ONERA M6, 2D section. Pressure contour levels for the original (left) and optimized (right) profiles.

5 Numerical examples

In the following examples, we apply the proposed method to three geometries of different complexity. The first two are rather academic: an ONERA M6 wing, which in fact **it is**

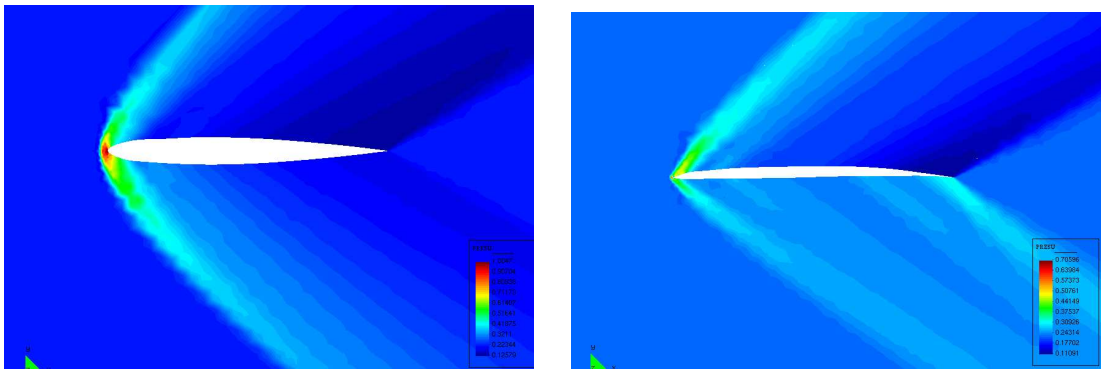

Figure 3: ONERA M6, 2D section. Pressure contour levels for the original (left) and optimized (right) profiles (blow-up).

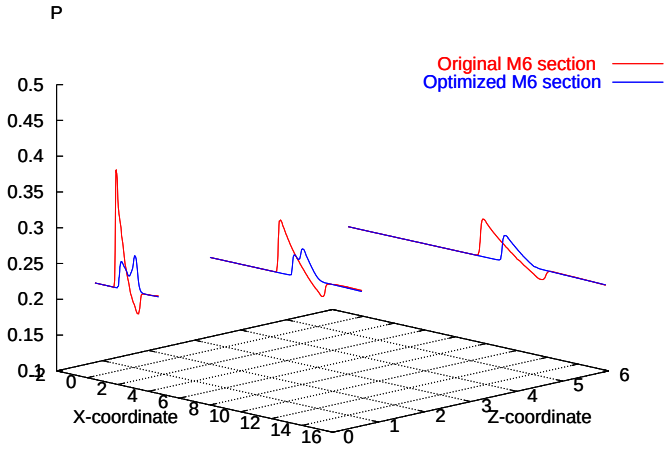

Figure 4: ONERA M6, 2D section. Pressure shock propagation below the airfoils at three different vertical positions placed at 0.5 , 3 and 6 chord lenghts (this is the Z-coordinate).

not a supersonic wing but it is very useful to test the scheme, and an aircraft's generic nose, built simply by rotating a NACA 0012. The last one is a shape of a future supersonic business jet, projected by Dassault Aviation.

5.1 ONERA M6 wing

Although the space discretization of this example is very coarse (2203 nodes, 10053 tetrahedra), it will thoroughly illustrate the ideas presented above. The wing's skin mesh is composed of 780 nodes, resulting in 1524 triangles. We have used this case to tune different parameters of the scheme. The initial conditions are defined by a farfield Mach number of 1.8 and an angle of attack of 3.00 degrees. The pressure distribution in the downwards wing face is seen in the Figure 5. Note in this Figure the coarseness of the mesh.

In this example, we have tested many different possibilities to carry out the shape optimization process. We have varied the parameters α_1, α_2 and α_3 of (13), and we have studied both the volume preserving gradient projection (VPGP) or the multilevel (additive or not) preconditioned method. In this case, we have seen that being the skin mesh so coarse, the additive multilevel preconditioner is unnecessary. The chosen α's parameters are: $\alpha_1 = 0$, $\alpha_2 = 1$ and $\alpha_3 = 10$, meaning that firstly, the drag is excluded from the cost functional, and secondly, its pressure gradient term is ten times "heavier" than the lift one.

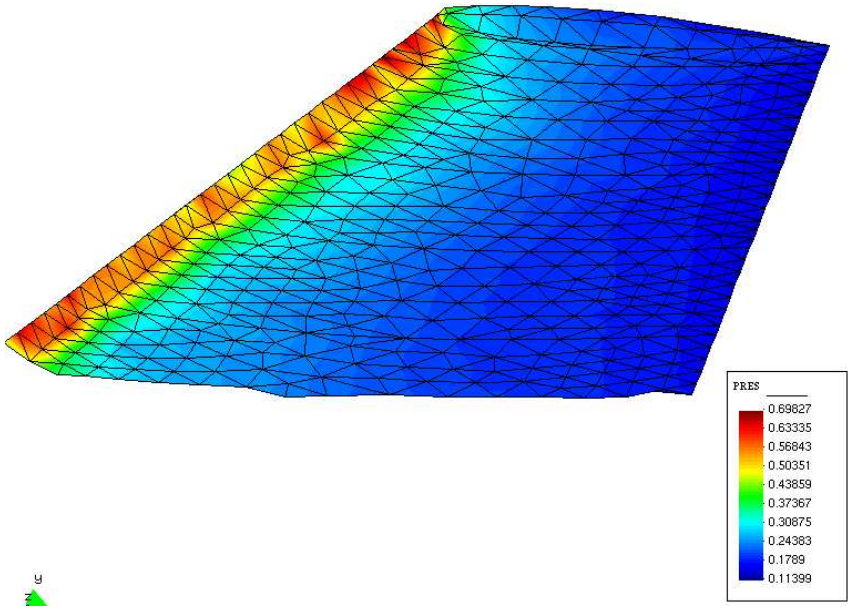

Figure 5: ONERA M6 wing. Pressure distribution of the downwards wing face, showing also the skin mesh.

Figure 6 shows two different optimized shapes, with and without VPGP optimization. In both cases, the downwards wing face is flattened, seeking to low down the sonic boom emission. Also the trailing edge is slightly curved downwards to conserve lift force. In the first case, with VPGP the volume lost in the face below is recovered in the face above, resulting in an optimized wing with the (approximately) the same volume. Whithout VPGP, the resulting wing is indeed finer and more efficient in general terms. The boom reduction is seen in Figure 7. It shows the pressure distribution along a line below the wing at half of its wingspan. The original M6 produces the typical Witham's F-function to the shock first strong compression, it follows first a strong over-expansion and then a smoother pressure recovery. As reported in works like [16], the N-shape, when propagated downwards, projects on the soil the sonic signature, which is the cause of the sonic boom for this particular case. We have seen above, in the 2D simplification for the M6 that this fact starts to become apparent at around 6 chord lengths below. The VPGP optimized wing smooths the N-shape, both by reducing the peak almost to half of its intensity and by retarding its rising. This fact produces a second advantage: the following expansion is shallower. But when the volume preserving constraint is unleashed, the resultant non-VPGP optimization yields a different, more extreme outcome: the bow shock projected donwards has disappeared, leaving a pressure "plateau", preceded by a smooth rising and followed by an also smooth expansion, with no trace of the N-shape. This is caused by the flattened down-face, which developes a more constant pressure distribution. The lift and drag coefficients for our original M6 and for both optimizations are shown in Table 1.

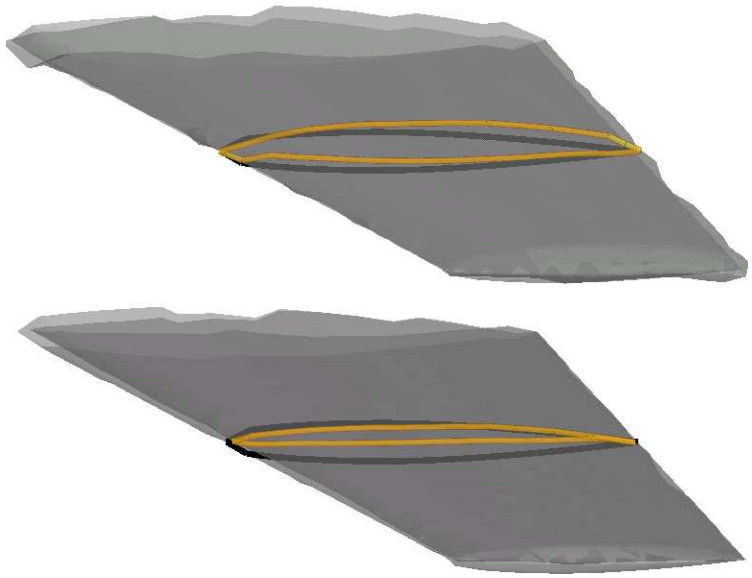

Figure 6: ONERA M6 wing. Optimized shapes. Top, with VPGP. Bottom, wihtout VPGP.

	Original	VPGP	no VPGP
C_L	0.0570	0.0348	**0.0556**
C_D	0.0319	0.0225	**0.0083**

Table 1: ONERA M6 wing. Drag and lift coefficient for VPGP (volume preserving gradient projection) and no-VPGP optimizations.

For this particular case, not keeping the volume constant has given a better outcome, because additionally, its aerodynamic performance is better: it has rendered a wing with a lift coefficient only 3% lower with half of the original wing thickness. Below it is shown that a different set of α's can produce shapes that while keeping the target aerodynamical properties and reducing the sonic boom emission, the preserve approximately the original volume.

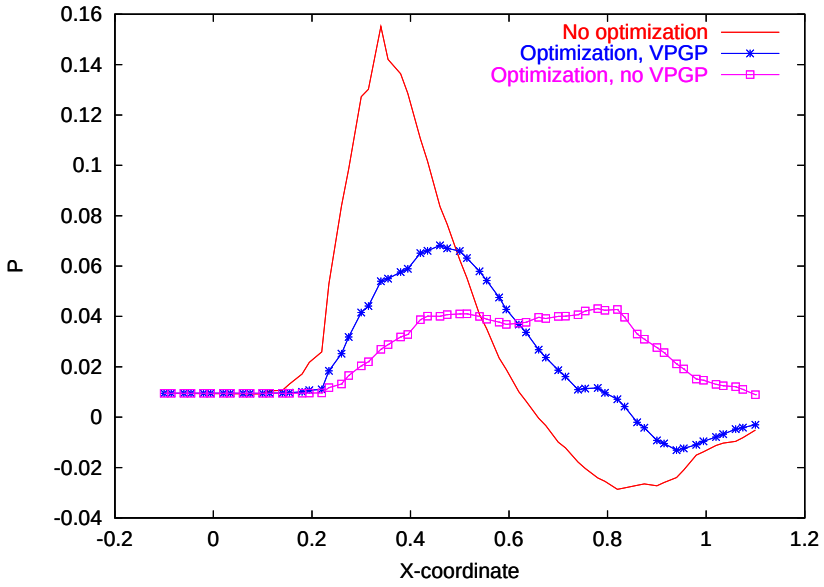

Figure 7: ONERA M6 wing. Pressure along a line below the wing.

5.2 Aircraft's generic nose

The flow regime is again $M = 1.8$. The geometry in this example was generated by rotating a NACA 0012 profile around its axis to produce an aircraft's nose-like form. The backwards facing part of the solid produced by the profile's rotation is replaced by a cylinder. The idea

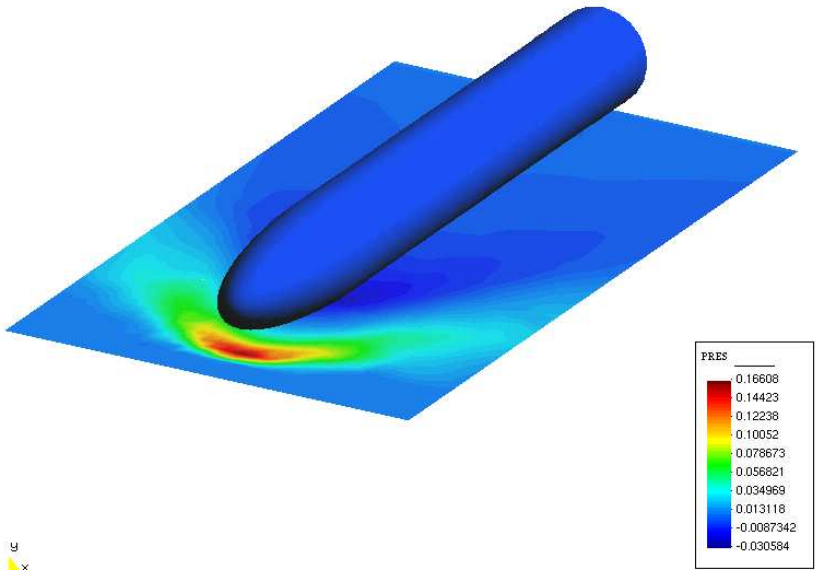

Figure 8: Aircraft's Generic Nose. Pressure distribution in a plane below the nose.

of this example is to show the effect of the sonic boom emission optimization acting alone on a simple geometry. The lift and drag terms in the cost functional are then eliminated by fixing $\alpha_1 = 0$ and $\alpha_2 = 0$, being $\alpha_3 = 1$. The optimization was done with VPGP on the complete volume. The spatial mesh is made of 57159 tetrahedra, comprising 11044 nodes. The skin mesh is made of 3316 triangles.

Figures 8, 9 and 10 show the effect of the optimization process. In this case, we have used the additive multilevel preconditioner and an additional smoothing for the cost functional gradient on the surface. The pressure distribution on the horizontal plane below the nose shows that the smoothening of the peak produced by the shock ahead the nose is very effective. This is achieved by prolonging the nose and rising the downwards half. The rising produces again a flattening of the part of the geometry which is facing down. As the full volume is conserved what goes ahead in the nose's optimized shape is compensated by what comes to the rest of the cylinder. This flattening is sharply finished at the trailing part of the cylinder, far from the nose, simply because there ends the numerical domain and those nodes are fixed. The resulting bump in the geometry produces the pressure expansion in the far right of the pressure plot in Figure 9. Anyway, this part of the domain is out of the optimization problem. In the next example, the VPGP done per-sections will probe effective to avoid this. The pressure plot in Figure 9 corresponds to the pressure distribution along the midline of the plane shown in Figure 8. It shows that, as in the case of the M6,

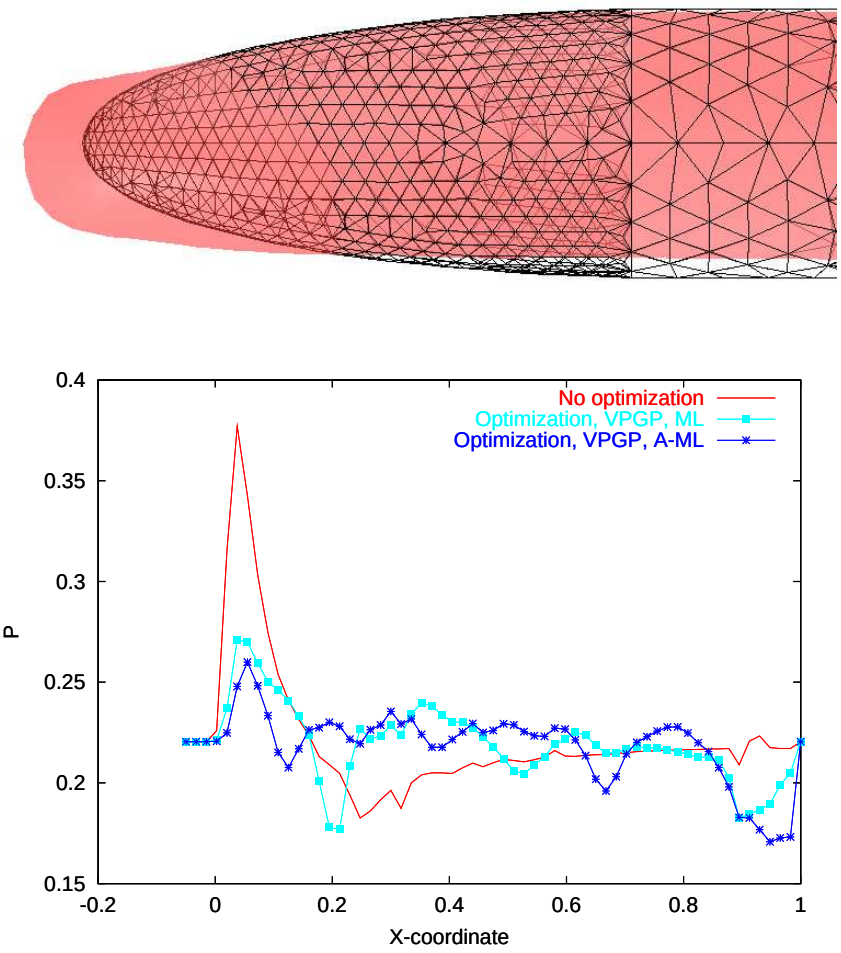

Figure 9: Aircraft's Generic Nose. Top, original geometry (mesh shown) and optimized shape (solid). Bottom, pressure along a centered line below.

after optimization the N-shape pressure is modified by a peak reduction and a rising of the posterior expansion, resulting in a more plane pressure distribution. In the plot, the results not using the preconditioner are also included, showing the substancial improvement of the additive multilevel, both in the peak and expansion reductions and in the smoothness pressure distribution downstream. Its jagged character is due to the coarseness of the surface

grid downstream the nose itself. The final outcome is not a complete shock flattening due to the grid coarseness but it shows a strong tendency towards it.

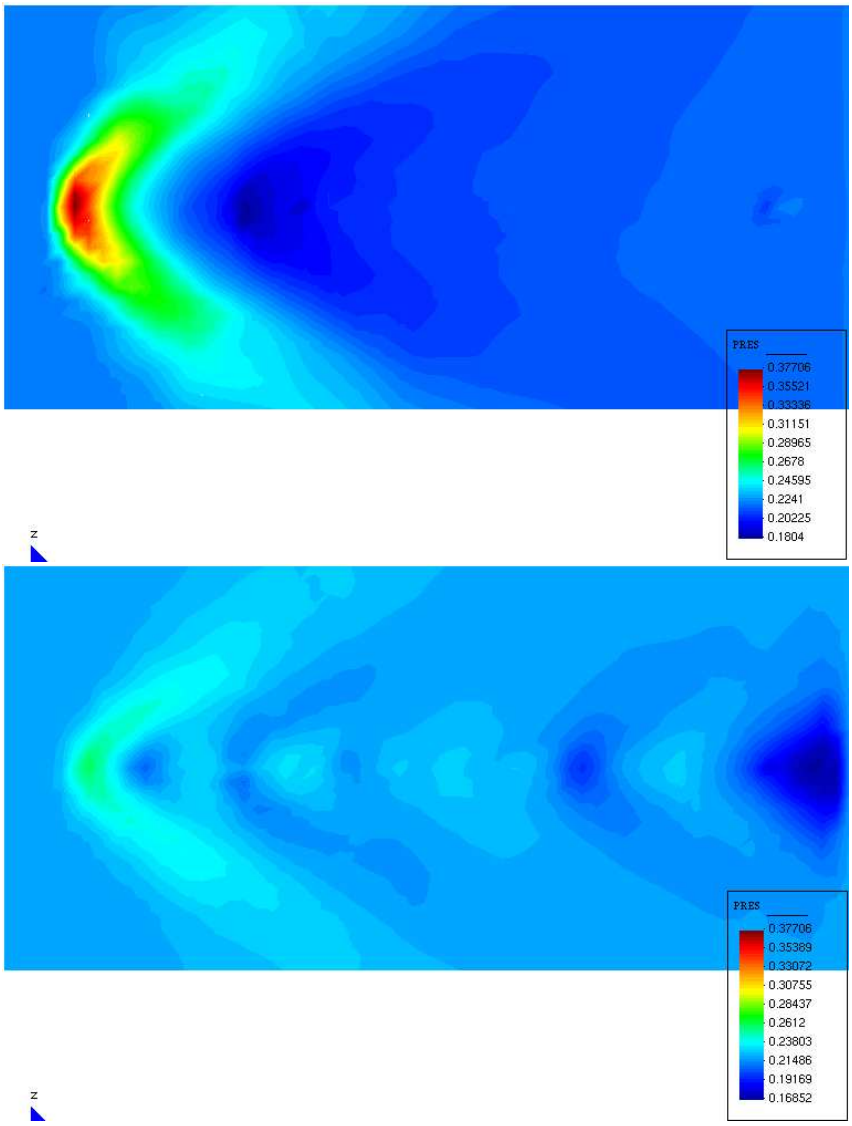

Figure 10: Aircraft's Generic Nose. Pressure distribution in a plane below the nose. Top, before optimization. Bottom, after optimization.

5.3 Supersonic Business Jet

The final example is an optimum design study done on a projected Supersonic Business Jet, under developement at Dassault Aviation. The geometry was provided by the constructor. The spatial grid has 173526 nodes in 981822 tetrahedra and corresponds to half of the aircraft, with a vertical symmetry plane (see Figure 11). The inflow Mach number is 1.8 and the angle of attack is 3°.

The aircraft wings are the targets of the optimization. The simplified wings provided by the constructor for this generic geometry are horizontally symmetrical, with two different sweep angles of 17° and 38° respectively, and a rather smooth transition between them. The Mach angle for $M = 1.8$ is around 34°. Therefore, while the inboard part of the wings falls within the Mach cone (viz. [2]) with no shock wave ahead and a lower wave drag, the outboard wing cut through the Mach cone. As a consequence, the shocks will be produced ahead of the *outboard* portion of the wing.

This study was carried out in two steps, described in the next sub sections. Firstly, the aircraft wings are extracted from the plane, re-meshed with a coarser skin mesh, and optimized. In this way, the wings are totally isolated of the influence of the rest of the fuselage. Like in the case of the M6 wing, a similarly coarse grid is used to do a preliminar study of the problem, which is now more complex due to the dual-sweep angle. In this case we will show the effect of the cost functional three constitutive terms. Secondly, we proceed to optimize the wings, but now integrated to the plane as in the original geometry. The objective is clear: what is the influence of the fuselage in the wings optimization process? Have the shapes obtained the same form? Is it necessary then, not only to consider the whole plane, but also to optimize it as a whole? Or maybe adding some specific parts of the fuselage? Figure 20 is clear: it shows the cost functional gradient distribution for the complete aircraft's surface at the initial optimization step. It tells which parts of the skin of the complete aircraft should be modified related to the sonic boom emission reduction. Combined with the isolated wings study, this could become a useful tool for the aircraft designers.

5.3.1 Isolated wings: wing optimization

The skin mesh is shown in Figure 12, top, that also shows the four cuts of Figure 14. The very coarse skin mesh comprises 2409 nodes. In the same figure, at the bottom, it can be seen the wing and the plane below, which is at the top of the control box. The pressure distribution on this plane is used in Figure 13 to check how effective the sonic boom emission reduction is. We have followed two different optimization strategies in order to see the influence of the sonic boom reduction related to the lift and drag cost functional terms, using two different sets of parameters α, shown in Table 2: **Optimization Strategy I** and **Optimization Strategy II**. In both cases, we seek to keep the drag and lift targets while reducing the sonic boom emission. The difference lays in the relative weight we assign to each of the terms in the cost functional. While the first strategy (I) enforces the aerodynamic performances, the second one is more aggressive facing the sonic boom emission (II). For both of them

we show the pressure distribution in the reference plane below, the wing profile at the four reference sections and the pressure distribution along a line below them.

	α_1 (weighting C_D term)	α_2 (weighting C_L term)	α_3 (weighting $\|\nabla p\|^2$ term)
Optimization Strategy I	1.0	10.0	0.001
Optimization Strategy II	1.0	10.0	0.1

Table 2: Isolated wings of the Supersonic Business Jet. Optimization strategies shown.

The pressure distribution below the wing after optimization clearly shows the two zones into and out of the Mach cone, and the differences of both of the optimization strategies. In the outboard region, the shock is reduced, its top flattened and the rear over-expansion is almost eliminated, as seen in Figure 14. Although strategy II seems to be more effective in the pressure peak reduction, both of them eliminate the over-expansion equally well. Strategy I produces a more uniform pressure distribution (see Figure 13), particularly in the inboard wing (see Figure 14, below sections C and D). Evidently, all this effects are not at all seen in a wing like the M6, for it lays all outside the Mach cone. Therefore, this study renders totally new wing shapes that are not uniformly modified by the optimization cycle along the wingspan direction, as seen in the airfoils obtained in sections A, B, C and D (Figures 15 and 16).

Figures 15 and 16 show the original and the optimized airfoils obtained when cutting the wings in the four sections of Figure 12. Both the optimization strategies shown here include a VPGP technique. As said above, in order to prevent outboard-to-inboard mass migration, the volume preserving gradient is evaluated by dividing the wing-span in, say, 30 sections and keeping the volume constant within each of them. For both strategies I and II, outboard and inboard optimized airfoils show a very different effect. As within the Mach cone there is no shock production, the two inboard airfoils do not develop an acute leading edge. Although their downwards sides are flattened, the leading edge remains blunt. On the other hand, the outboard optimized airfoils present very acute leading edges, particularly for the closest one to the wing tip. Strategy II tends to create more flattened outboard wing sections and more cambered inboard ones, due to its more aggressive effect on pressure peak reduction. Because of the volume preservation, this is translated in an outspread of the upper wing side, particularly in its rear part. On the other hand, the shape produced

by Strategy I is smoother, because as the flattening and cambering of the downwards wing side is less, the upper side is also more uniform. This effect is in turn seen as a pressure overall flattening in the reference plane below the aircraft, as seen in Figure 13. We believe that this effect is equivalent to the pressure "plateau" in Figure 4. It is remarkable that for both strateties I and II, the inboard optimized shape present the same tendency as that of [6], where only drag and lift are included in the optimization cost.

The most important difference in the results produced by Strategies I and II is *not* seen in the sonic boom donwards emission, which is reduced almost equally well in both cases. What in fact set the differences are the aerodynamical wing properties, as shown in table 3: Optimization Strategy I leaves the aerodynamical performances almost intact.

	C_D	C_L	C_L/C_D
Original	0.011	0.057	5.18
Optimization Strategy I	**0.011** (target 0.0)	**0.056** (target 0.057)	5.09
Optimization Strategy II	0.012 (target 0.0)	0.051 (target 0.057)	4.25

Table 3: Isolated wings of the Supersonic Business Jet. Optimization strategies shown.

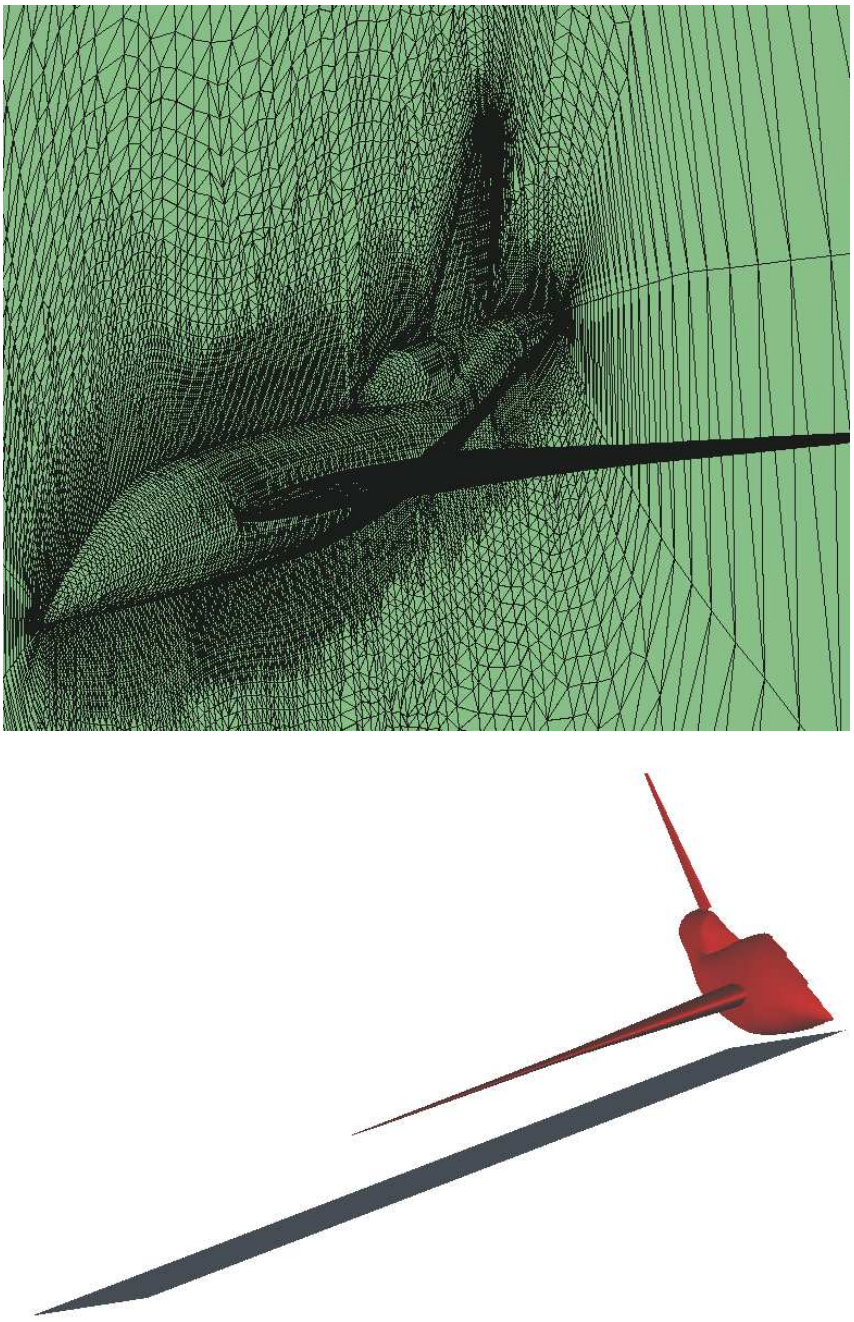

Figure 11: Dassault's Supersonic Business Jet. Top, spatial grid close-up. Bottom, aircraft and reference plane below.

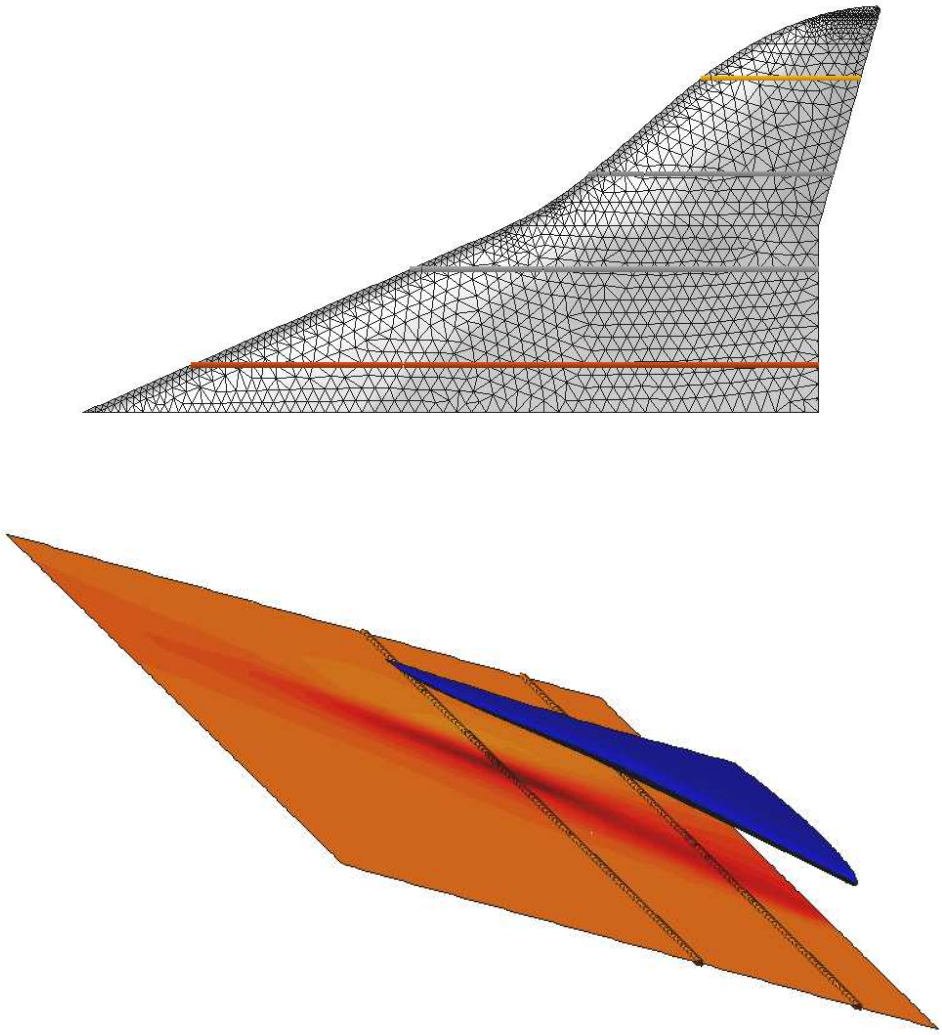

Figure 12: Isolated wings of the Supersonic Business Jet. Top, wing skin mesh and its four sections considered (the thick horizontal lines), named sections A, B, C and D from outside going inside towards the fuselage. Bottom, wing and reference plane below.

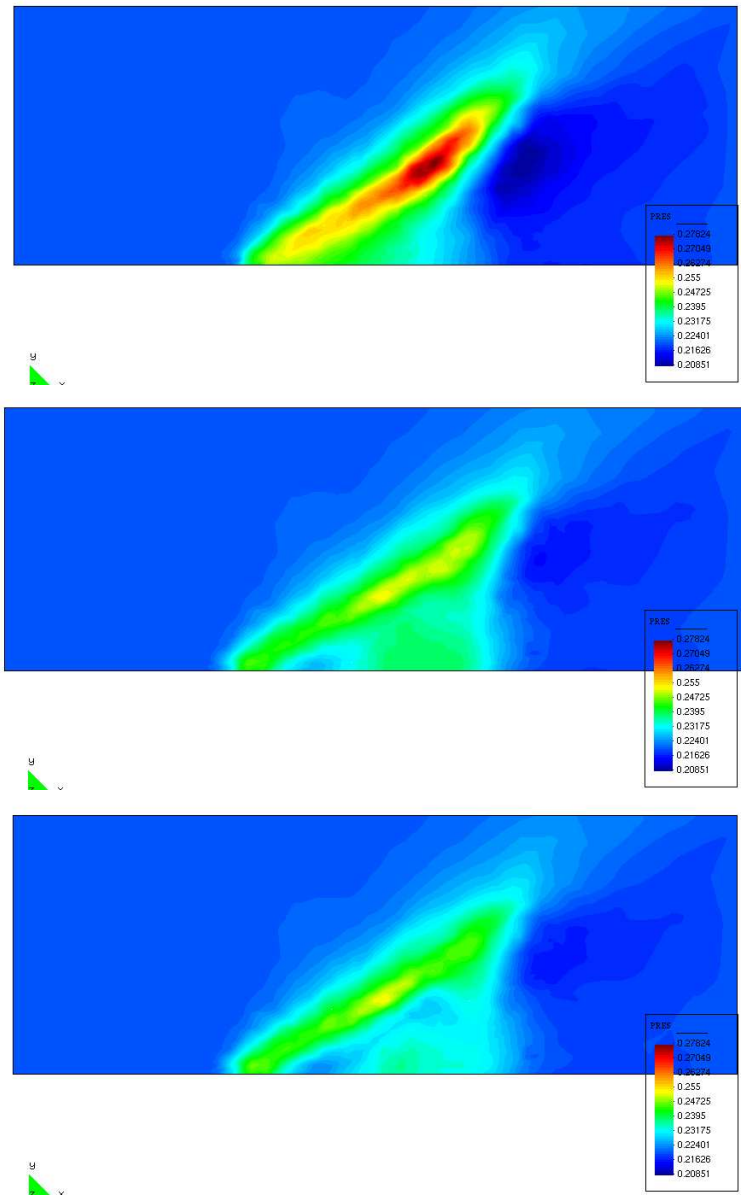

Figure 13: Isolated wings of the Supersonic Business Jet. Pressure distribution in the reference plane below the wing. Top, original geometry. Mid and bottom, optimized geometries following strategies (I) and (II) respectively.

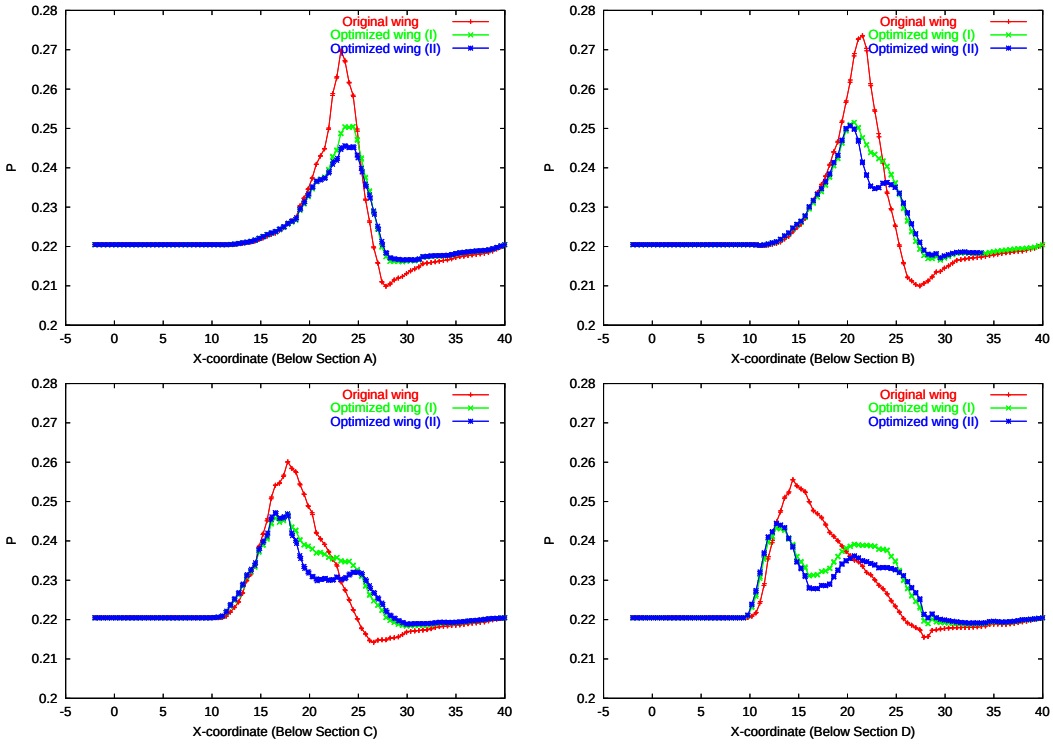

Figure 14: Isolated wings of the Supersonic Business Jet. Pressure along the lines projected by sections on the reference plane below the aircraft.

Figure 15: Isolated wings of the Supersonic Business Jet. Optimization Strategy I. Shape optimization shown at the four wing sections. From top to bottom: Sections A, B, C and D. In blue, the original shape.

Figure 16: Isolated wings of the Supersonic Business Jet. Optimization Strategy II. Shape optimization shown at the four wing sections. From top to bottom: Sections A, B, C and D. In blue, the original shape.

5.3.2 Integrated airplane: wing optimization

The study continues with the complete airplane, of which Figure 17 shows the Mach number and pressure distribution over the surface of the whole aircraft. [1] Now, again only the wings are optimized but the influence of the rest of the plane is taken into account: it is deduced from the results that it is not at all negligeable.

The outcome of 8 optimization cycles is shown in 18. In this figure it can be seen that the main peak has indeed diminished, as in all the other cases. Like when the wings were optimized isolatedly, the optimization procedure has managed to dump the shock produced by the part of the wing which is out of the Mach cone (19, top). However, within the Mach cone, the pressure peak has augmented after the optimization (19, bottom). Slightly augmented indeed, because its maximum remains close to that of the reduced shock. We believe that this fact can be attributed to the effect of the rest of the aircraft, especially the neighboring fuselage. As seen in 20, the cost functional gradient distribution for the complete aircraft's surface tells us which parts of the skin of the complete aircraft should be optimized relatively to the cost functional proposed here. As a morale from the application of out technique to this example, it can be said that the optimization of the isolated aircraft parts could give deeper ideas to the designer on where are located the problems, even for rather coarse skin meshes. This optimization can be done much faster than that of the full aircraft and several different forms can be produced and tested until some of them are selected. This changes can be introduced in the full aircraft, and ultimately optimized completely to assess the changes.

[1] However, results figures show the complete aircraft. This is due only to a postprocessing trick, which uses the symmetry plane as a "mirror". This leads to a better and easier results interpretation.

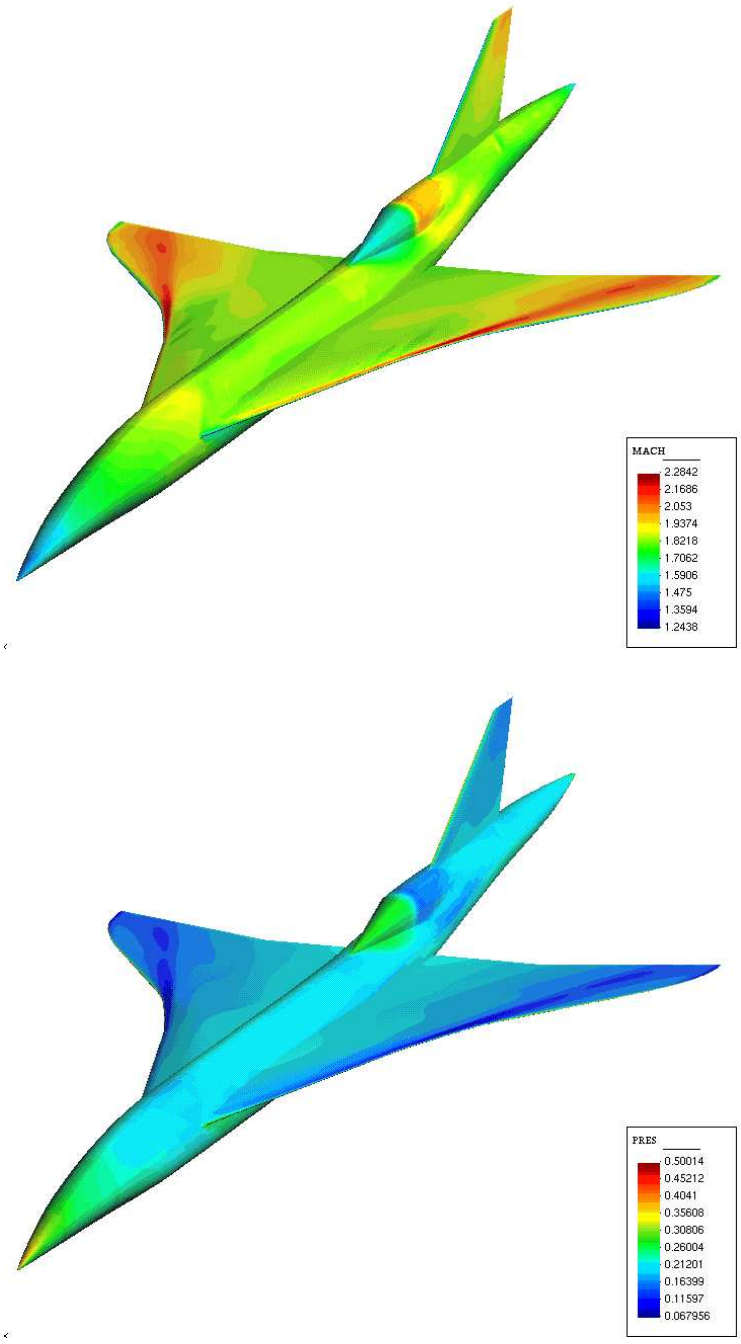

Figure 17: Supersonic Business Jet. Contour levels. Top, Mach number. Bottom, pressure.

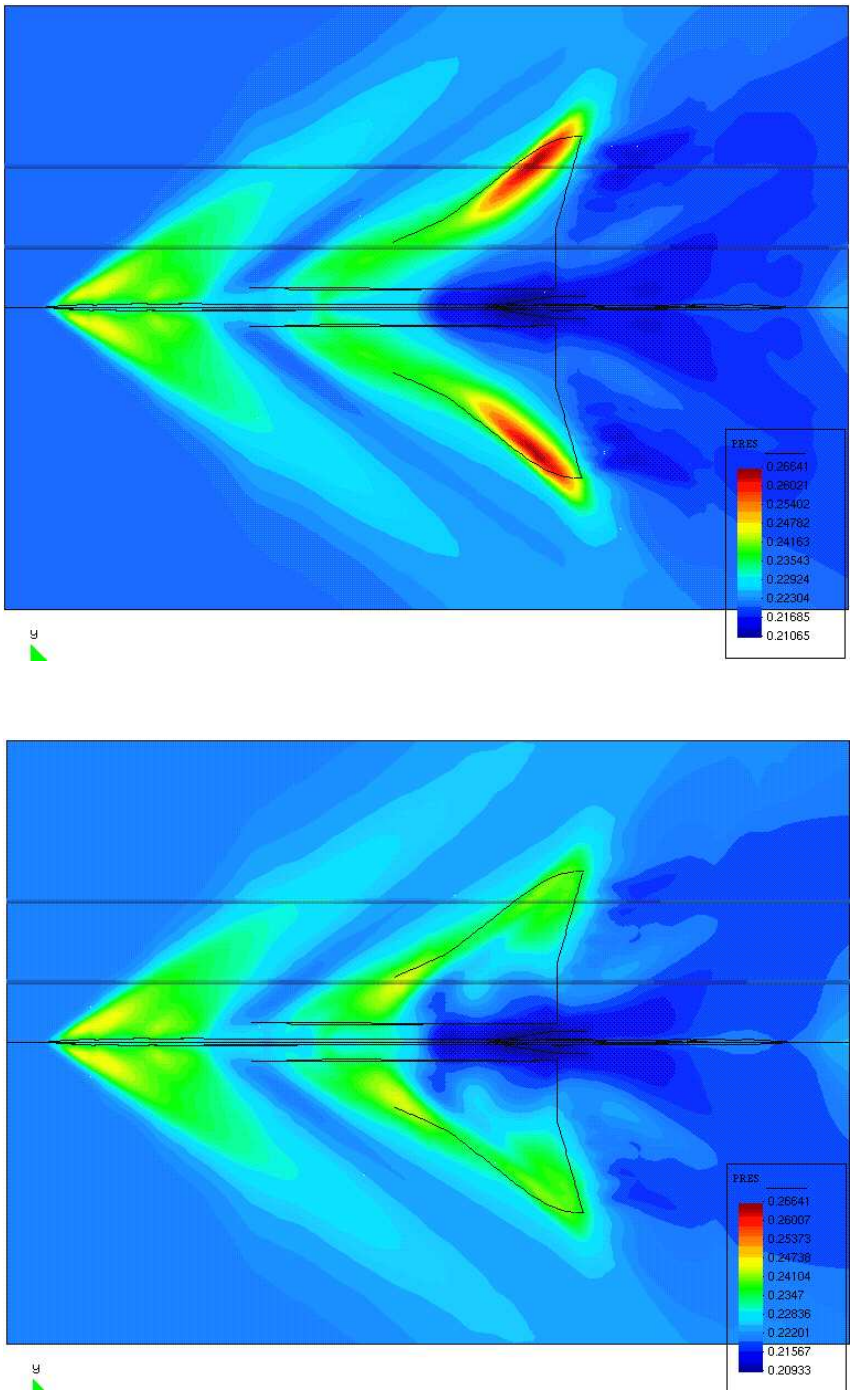

Figure 18: Supersonic Business Jet. Pressure distribution in a plane below the aircraft. Top, original geometry. Bottom, optimized geometry. The two lines of Figure 19 are shown here.

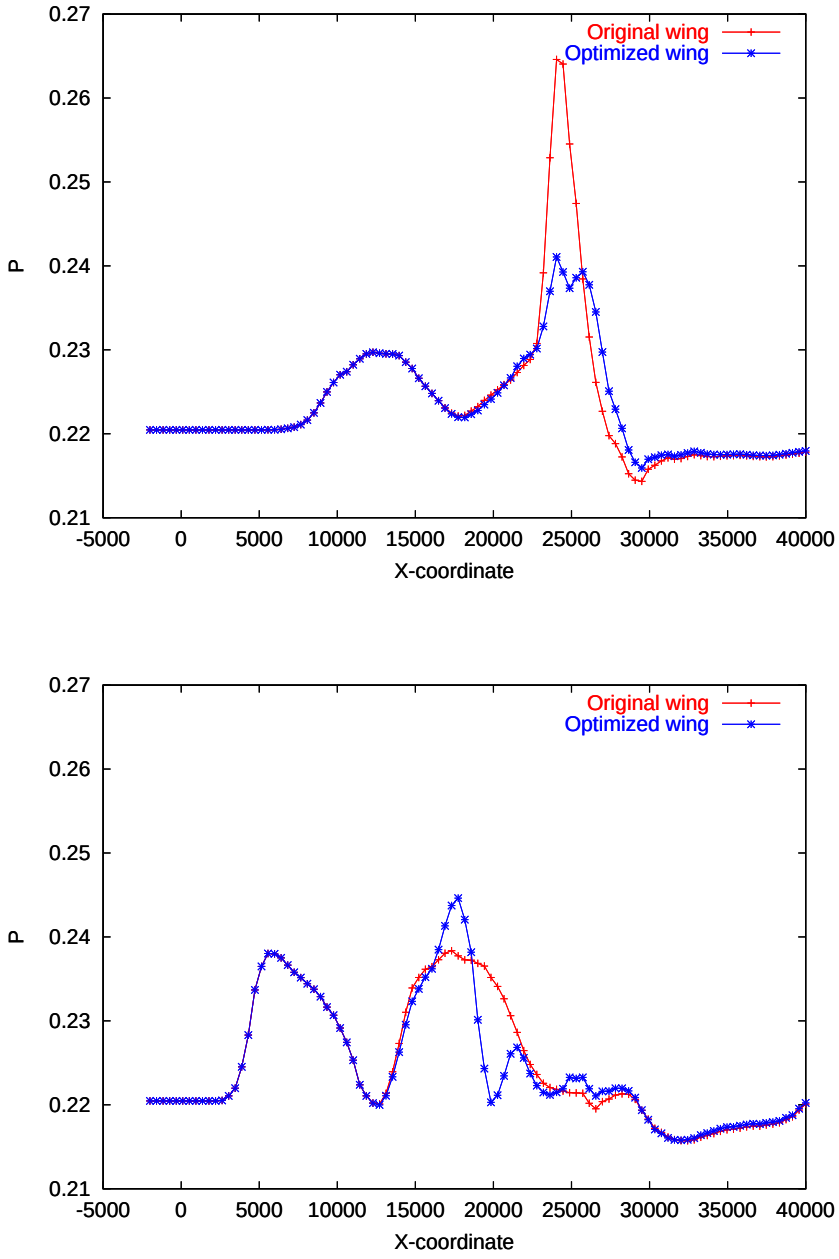

Figure 19: Supersonic Business Jet. Pressure along two lines below the wing, outside (top) and inside (bottom) the Mach cone.

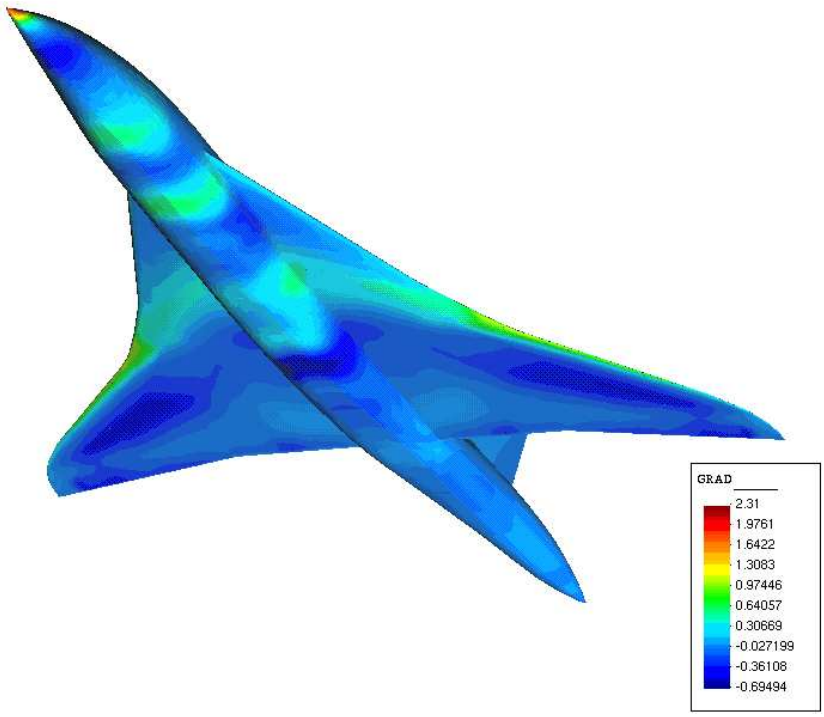

Figure 20: Supersonic Business Jet. Cost functional gradient distribution for the complete aircraft's surface.

6 Conclusion

We have proposed a new method for the optimization of aerodynamic shapes, which is based mainly in two original ideas. First, and from a mathematical point of view, the extension of an additive multilevel method is applied to 3D shape parametrization. The shapes so obtained are smoother and convergence rates are faster than when no preconditioner is present. This technique is also combined with several options well adapted to each other: CAD-free parametrization to work on the discretized shapes, Euler flow model with transpiration conditions which simulates the shape modifications produced by the optimization process, or a discrete adjoint approach, to deal with the eventually large dimension of the design variables space (up to 11000 surface grid points for the full Supersonic Business Jet fuselage optimization).

Laying on the optimum design side, the second original concept is the sonic boom optimization in itself. It is based on two pilars: *what* we in fact reduce and *how* we manage to reduce it. On the one hand, we are not trying to reduce the sonic boom itself (i.e. the shock signature on the soil, in the far field), what requires additional simulations out of the Euler flow equations scope. Instead of this, our goal is to reduce the pressure shock intensity in the near field below the plane, what we have called the sonic boom emission. On the other hand, we do it by modifying the aerodynamic shapes themselves. The parameters space is then the physical position of the skin mesh nodes, a mesh that in turn can be adapted to the needs of the flow field.

Although the sonic boom emission is addressed in a simplified but effective manner, the shape optimization technique here proposed allows to conduct the research among a very large family of shapes. Very simple examples show that bang-free geometries exist when no lift constraint is required, a well known fact: lift produces sonic boom that will be always there [27]. So when lifting bodies are seeked, shapes with flattened downards halves play a particularly interesting role since in many cases they produce low sonic pressure rises, while keeping the lift. These kind of shapes are well reproduced by the algorithm here proposed. We illustrate this point with a series of optimization examples with increasing shape complexity, rising up to a pre-industrial jet geometry. Additionally, the scheme here proposed provides enough flexibility to tune the desired aerodynamic properties against the sonic boom downards emission.

There are still several limitations in the accuracy of our results, that lead the way to future lines of research. First, a spatially second-order accurate adjoint is currently under development. Then, the inaccuracy induced by the transpiration based modelisation of large shape modifications will be supposedly controlled by the regeneration of a genuine mesh following the optimal shape. Studies in this direction have demonstrated that the final shapes obtained purely with transpiration do not change by further optimization after a domain remeshing is carried out, which takes as the new skin mesh the outcome of the transpiration conditions. This would suggest (at least for the problems studied) that transpiration is a valid option to deal with the shape modifications so induced. However, after the initial optimization steps performed only with transpiration, the resulting skin mesh can present excessive coarsening in regions where surface modifications has been important. Therefore

some kind of surface inlaying (coming from triangles division, for instance) should be considered in these regions before complete remeshing. A forthcoming paper will assess the 3D transpiration model by combining it with re-meshing.

Also the efficiency of the proposed approach can become an important issue when stiffer functional and constraints were considered and tenths of gradient iterations will be mandatory. Now, each iteration requires the complete solution of state and adjoint systems. In [7], we propose a new method inspired by SQP techniques for the simultaneous, or one-shot, solution of state, adjoint and optimality conditions. Concerning the cost functional presented here, we believe that although it has shown a very efficient performance, it can be further improved.

In a following paper, we keep on developing the scheme here presented, by going deeper and farther. Deeper, because we work on a spatially second-order accurate adjoint, obtained by automatic differentiation of the flow, that is in turn discretized using a Roe scheme. Also the transpiration conditions are first assessed and then combined with a remeshing technique. And farther because the next objective is to solve multiphysics problems by adding to the optimization cycle the aeroelastic coupling. In this way, the sonic boom optimization will take into account also the deformations suffered by the aerodynamic shapes due to aeroelastic effects.

Acknowledgements : We thank Dassault Aviation for making available his Supersonic Business Jet's mesh for this project, and particularly M. Mallet for reading and commenting this document. We are also grateful to CINES (Centre Informatique National de l'Enseignement Supérieur) for providing the computational facilities where the largest examples were ran and to the French Ministry of Research for granting the project, in the names of S. Candel and D. Jeandel.

References

[1] J. ALONSO, I. KROO, and A. JAMESON. Advanced algorithms for design and optimization of quiet supersonic platforms. *AIAA Paper*, 2002-0144:1–13, 2002.

[2] J. D. ANDERSON. *Introduction to Flight.* Mc. Graw - Hill, 2000.

[3] F. BEUX and A. DERVIEUX. A Hierarchical Approach for Shape Optimization. *Engineering Computations*, 11(1):25–48, February 1994.

[4] C. BISCHOF, A. CARLE, G. CORLISS, and A. GRIEWANK. ADIFOR : Automatic Differentiation in a Source Translator Environment. In Paul S. Wang, editor, *International Symposium on Symbolic and Algebraic Computation*, 1992.

[5] J.H. BRAMBLE, J.E. PASCIAK, and J. XU. Parallel multilevel preconditionners. *Math. Comp.*, 55:1–22, 1990.

[6] S.E. CLIFF, J.J. REUTHER, D.A. SAUNDERS, and R.M. HICKS. Single-point and multipoint aerodynamic shape optimization of high-speed civil transport. *Journal of Aircraft*, 38(6):997–1005, 2001.

[7] A. DERVIEUX, F. COURTY, M. VAZQUEZ, and B. KOOBUS. Additive multilevel optimization and its application to sonic boom reduction. In Finalnd. Jyvaskyla, editor, *Numerical Methods for Scientific Computing - JP60 Meeting. Variational Problems and Applications.*, 2002.

[8] A. DERVIEUX, S. LANTERI, J.M. MALE, N. MARCO, N. ROSTAING-SCHMIDT, and B. STOUFFLET. New technologies for advanced three-dimensional optimum shape design in aeronautics. *Int. J. Num. Meth. Fluids.*, 30:179–191, 1999.

[9] C. FARHAT, K. MAUTE, B. ARGROW, and M. NIKBAY. A shape optimization methodology for reducing the sonic boom initial pressure rise. *AIAA Paper*, 2002-0145:1–11, 2002.

[10] H. GUILLARD and N. MARCO. Some aspects of Multigrid Methods on Non-Structured meshes. In *Proceedings of the Conference of Copper Mountain on Multigrid Methods*, April 1995.

[11] W. P. HUFFMAN, R. G. MELVIN, D. P. YOUNG, F. T. JOHNSON, J. E. BUSSOLETTI, M. B. BIETERMAN, and C.L. HILMES. Practical Design and Optimization in Computational Fluid Dynamics. *AIAA Paper 93-3111*, 1993.

[12] T.J.R. HUGHES. *The Finite Element Method.* Prentice-Hall, 1987.

[13] G. KURUVILA, S. TA'ASAN, and M.D. SALAS. Airfoil Optimization by the One-Shot method. Aiaa paper, 1994.

[14] M.-H. LALLEMAND, H. STEVE, and A. DERVIEUX. Unstructured multiggridding by volume agglomeration : current status. *Computer and Fluids*, 21(3):397–433, 1992.

[15] J.-L. LIONS. *Contrôle optimal de systèmes gouvernés par des équations aux dérivées partielles*. Dunod Gauthier-Villars, 1968. (in French) Collection Etudes Mathématiques dirigée par P. Lelong.

[16] D.J. MAGLIERI and K.J. PLOTKIN. *Aeroacoustics of flight vehicles: theory and practice*. Acoustical Society of America, Publications, 1991.

[17] N. MARCO and F. BEUX. Multilevel optimization: application to one-shot shape optimum design. Research Report 2310, INRIA Sophia-Antipolis, October 1993.

[18] N. MARCO and A. DERVIEUX. Agglomeration method applied to the Hierarchical Parametrization of a Skin Mesh in 3D Aerodynamics, 1994. Contributions to 12th month of European Project ECARP.

[19] N. MARCO and A. DERVIEUX. Multilevel parametrization for aerodynamical optimization of 3D shapes. *Finite Elements in Analysis and Design*, 26:259–277, 1997.

[20] B. MOHAMMADI. Optimization of aerodynamic and acoustic performances of supersonic civil transports. In *Center for Turbulence Research. Proceedings of the Summer Program 2002*, 2002.

[21] B. MOHAMMADI and O. PIRONNEAU. *Applied shape optimization for fluids*. Clarendon Press - Oxford, 2001.

[22] G.D. MORTCHELEWICZ. Résolution des équations d'Euler tridimensionnelles instationnaires en maillages non structurés. *La Recherche Aérospatiale*, (6):17–25, Novembre-Décembre 1991.

[23] S. NADARAJAH, A. JAMESON, and J. ALONSO. An adjoint method for the calculation of remote sensitivities in supersonic flow. *AIAA Paper*, 2002-0261:1–15, 2002.

[24] N.MARCO, B. KOOBUS, and A. DERVIEUX. An Additive Multilevel Preconditioning Method. Research Report 2310, INRIA Sophia-Antipolis, August 1994.

[25] J. REUTHER and A. JAMESON. Aerodynamic Shape Optimization of Wing and Wing-Body Configurations Using Control Theory. AIAA Paper 95-0123, 1995. 33rd Aerospace Sciences Meeting and Exhibit.

[26] N. ROSTAING-SCHMIDT and S. DALMAS. Automatic analysis and transformation of fortran programs using a typed functional language. Technical Report 1518, INRIA Sophia-Antipolis, 1991.

[27] R. SEEBAS and B. ARGROW. Sonic boom minimization revisited. *AIAA Paper*, 98-2956:1–13, 1998.

[28] H. YAMAGUCHI and Y. NAKAMURA. Optimization of low boom configuration of SST by genetic algorithm. *AIAA Paper*, 98-2899, 1998.

Unité de recherche INRIA Sophia Antipolis
2004, route des Lucioles - BP 93 - 06902 Sophia Antipolis Cedex (France)

Unité de recherche INRIA Lorraine : LORIA, Technopôle de Nancy-Brabois - Campus scientifique
615, rue du Jardin Botanique - BP 101 - 54602 Villers-lès-Nancy Cedex (France)
Unité de recherche INRIA Rennes : IRISA, Campus universitaire de Beaulieu - 35042 Rennes Cedex (France)
Unité de recherche INRIA Rhône-Alpes : 655, avenue de l'Europe - 38330 Montbonnot-St-Martin (France)
Unité de recherche INRIA Rocquencourt : Domaine de Voluceau - Rocquencourt - BP 105 - 78153 Le Chesnay Cedex (France)

Éditeur
INRIA - Domaine de Voluceau - Rocquencourt, BP 105 - 78153 Le Chesnay Cedex (France)
http://www.inria.fr
ISSN 0249-6399